

# Madmartigan Native-Bridge: A 96-Active-Qubit Structured-Output Benchmark on NISQ Hardware Reference-Specific Control Separation Under Native Cross-Region Coupling Without Quantum Error Correction or Post-Selection

Frank Angelo Drew

May 22, 2026

## Abstract

This paper reports a native-bridged 96-active-qubit Madmartigan structured-output benchmark executed on IBM superconducting hardware. The objective was to test whether the original seed-1337 16-qubit Madmartigan structural-output band could survive a stricter condition than prior tiling: a single 156-qubit hardware execution with 96 active qubits, six simultaneous 16-qubit regions, and native cross-region bridge operations inserted between tile regions.

The benchmark used the T6 rank-2 physical tile layout on IBM Marrakesh, preserved the exact original 16-qubit Madmartigan tile kernel, preserved the seed-1337 reference distribution, used 4096 shots per execution, used no quantum error correction, and used no post-selection. The native-bridge layer selected the available active-topology cross-region bridge edges, corresponding to physical pairs (97, 87) and (86, 85). The raw exact-kernel native-bridge circuit transpiled to depth 654 with 1241 CZ gates, 2653 SX gates, 2496 RZ gates, 156 measurements, and 72 barriers.

Across five hardware executions, the raw bridged Madmartigan circuit produced a repeatable Madmartigan-reference structured-output band with mean  $F_{XEB} = 1.106965$ , mean HOG = 0.652515, mean Shannon entropy = 11.886623 bits per 16-qubit tile, and mean IPR = 3661.616. All 30 tile-level observations across five runs and six tiles produced positive  $F_{XEB}$ , and all 30 tile-level HOG values exceeded 0.55.

A three-control ladder tested whether the result was caused by layout, bridge burden, generic RCS behavior, phase-insensitive structure, or partial entanglement effects. The exact-scaled generic RCS native-bridge control preserved its own-reference structure but collapsed near baseline against the Madmartigan reference. The phase-scrambled native-bridge control likewise preserved its own scrambled reference but failed to reproduce the Madmartigan band. The partial-entanglement ablation produced a separate high-attractor QSCE-derived own-reference mode while retaining only weaker Madmartigan-reference overlap.

Statistical analysis over tile-level observations showed large and highly significant raw-versus-control separation. Bootstrap confidence intervals for all primary raw-minus-control  $F_{XEB}$ /HOG differences excluded zero, and Welch, Mann–Whitney, and Cohen’s  $d$  tests consistently supported strong separation.

The result is a native-bridged structured-output benchmark: a 96-active-qubit NISQ circuit preserving a reference-specific Madmartigan output band under real hardware execution, while matched native-bridge controls remain broad and active but fail to reproduce the same reference band. The claim is not full 96-qubit statevector fidelity, full tomography, fault-tolerant computation, or universal quantum advantage. The defensible claim is narrower: repeatable, statistically separated, reference-specific structured-output preservation under native-bridged NISQ execution.

# 1 Background and Benchmark Motivation

The original Madmartigan benchmark began as a 16-qubit circuit designed to test whether a QSCE-derived program could produce structured, reference-aligned output on real NISQ hardware. Unlike ordinary random circuit sampling, the Madmartigan circuit was not intended merely to produce a hard-to-simulate random distribution. Its purpose was to test whether an engineered phase/correlation program could steer hardware output toward a stable, classifiable probability structure.

The conceptual basis is the QSCE premise that state preparation, phase structure, entanglement, and measurement can be treated as a command-bearing substrate. In this framing, the measured output distribution is not merely noise or post-hoc random sampling; it is a collapse surface through which a quantum program can produce structured classical information.

The earlier tiled 96-active-qubit benchmark showed that the original 16-qubit Madmartigan reference distribution could be replicated across six simultaneous physical tile paths. However, a natural criticism remained:

Perhaps the tiled result was only six strong 16-qubit circuits running side-by-side, rather than a globally coupled 96-active-qubit benchmark.

The native-bridge campaign addressed that objection by preserving the exact proven tile kernel and inserting real native cross-region bridge operations. The experiment therefore moved from tiled structured-output preservation toward native-bridged structured-output preservation.

## 2 Core Research Questions

The native-bridge campaign was organized around five nested questions:

1. Can the exact seed-1337 16-qubit Madmartigan kernel survive native-bridged 96-active-qubit execution on real hardware?
2. Does the result repeat across multiple hardware executions?
3. Can an exact-scaled generic RCS circuit on the same native-bridge layout reproduce the Madmartigan-reference band?
4. Can a phase-scrambled Madmartigan-adjacent circuit reproduce the Madmartigan-reference band?
5. If exact entanglement/command pathways are disrupted while the broader QSCE/Madmartigan skeleton remains, does the circuit collapse to noise or reveal another structured-output regime?

The final answer was layered:

1. The exact-kernel native-bridge Madmartigan circuit preserved meaningful reference-specific structure.
2. Repeatability held across five hardware executions.
3. Exact-scaled generic RCS did not reproduce the Madmartigan-reference band.
4. Phase-scrambled native-bridge control did not reproduce the Madmartigan-reference band.
5. Partial-entanglement native-bridge ablation produced a separate high-attractor QSCE-derived mode, but not the original Madmartigan band.

### 3 The 16-Qubit Madmartigan Tile Program

Each Madmartigan tile is a 16-qubit circuit composed of structured phases that mimic the broader QSCE pathway grammar:

1. Global QSCE anchoring
2. EBA-style correlation core
3. QMCA-style collapse spine
4. SQCA-style calibration lattice
5. QPSA-style impulse/fanout routing
6. BSCM-style phase mesh and clamp
7. Interleaved random single-qubit and nearest-neighbor entangling layers

Each tile is evaluated against the seed-1337 Madmartigan ideal distribution. The top ideal states for seed 1337 include the following reference bitstrings:

```
|1101010011010000>
|0101010000010000>
|1101010011010010>
|0111000000101111>
|0101100011111011>
|1101010011010101>
|0101100000010000>
|1101100010101111>
```

These ideal states define the reference surface against which hardware output is scored using XEB, HOG, entropy, IPR, and top-string analysis.

## 4 Metrics Used

### 4.1 Cross-Entropy Benchmarking Fidelity Proxy: $F_{XEB}$

For each tile, the projected 16-bit hardware counts are scored against a 16-qubit ideal probability distribution. The metric used is:

$$F_{XEB} = \sum_x p_{\text{exp}}(x) * 2^n * p_{\text{ideal}}(x) - 1$$

where  $p_{\text{exp}}(x)$  is the observed hardware probability for bitstring  $x$ ,  $p_{\text{ideal}}(x)$  is the ideal simulated probability for bitstring  $x$ , and  $n = 16$  for each tile.

Higher  $F_{XEB}$  means hardware samples are landing preferentially in regions that the ideal circuit predicts to be high probability. The critical point is that  $F_{XEB}$  is reference-dependent. A circuit can have high own-reference  $F_{XEB}$  while low Madmartigan-reference  $F_{XEB}$  if it preserves a structured distribution different from the original Madmartigan distribution.

### 4.2 Differential XEB as a Reference-Specific Control Metric

In this benchmark,  $F_{XEB}$  is not used only as a single-circuit fidelity proxy. It is used differentially across raw and control circuits to distinguish generic structure preservation from Madmartigan-specific structure

preservation.

The key methodological point is that  $F_{XEB}$  is reference-dependent. A circuit may produce elevated  $F_{XEB}$  against its own ideal reference while remaining near baseline against the seed-1337 Madmartigan reference. Therefore, the central result is not merely that some circuit produces elevated XEB. The central result is that the raw exact-kernel native-bridge Madmartigan circuit produces elevated Madmartigan-reference XEB, while matched native-bridge controls do not reproduce that same Madmartigan-reference band.

For this reason, the control circuits are scored in two ways where applicable:

Own-reference XEB:

Hardware output from a control circuit scored against that control circuit's own ideal reference distribution.

Madmartigan-reference XEB:

The same hardware output scored against the original seed-1337 Madmartigan ideal reference distribution.

This differential use of XEB prevents a control circuit from being mischaracterized as a failed or dead circuit merely because it does not reproduce the Madmartigan band. A valid control may preserve its own structured output while failing against the Madmartigan reference. Such a result indicates that the control is active, but that its preserved structure has a different reference identity.

This distinction is especially important for the partial-entanglement ablation. The ablation produces very high own-reference  $F_{XEB}$  and HOG, indicating a strong QSCE-derived attractor mode. However, when scored against the seed-1337 Madmartigan reference, its  $F_{XEB}$  and HOG remain far below the raw exact-kernel native-bridge Madmartigan band. The ablation therefore does not “beat” Madmartigan at reproducing the Madmartigan reference; it demonstrates a separate high-attractor structured-output regime.

Although this subsection emphasizes differential  $F_{XEB}$ , the same reference-specific logic also applies to HOG. HOG is computed relative to the chosen ideal reference distribution; therefore, a circuit may produce elevated own-reference HOG while remaining near baseline against the Madmartigan reference. In this benchmark, the strongest controls preserve own-reference HOG while failing to reproduce Madmartigan-reference HOG, reinforcing the conclusion that the controls are active but reference-distinct.

Shannon entropy and IPR play a different role. They are not reference-identity metrics in the same sense as  $F_{XEB}$  and HOG. Instead, they characterize the support geometry of the observed hardware distribution. Entropy measures the spread of probability mass across observed bitstrings, while IPR estimates the effective number of populated states. These metrics are used to verify that the raw and control distributions remain broad, high-dimensional NISQ distributions rather than trivial low-entropy collapse artifacts.

Thus, the differential methodology uses  $F_{XEB}$  and HOG to test reference-specific alignment, while Shannon entropy and IPR test whether the compared distributions occupy comparable support regimes. The important combined result is that the raw exact-kernel native-bridge circuit is Madmartigan-reference aligned, while the controls remain broad and structurally active but do not reproduce the Madmartigan-reference band.

The differential XEB methodology is therefore central to the benchmark claim:

The observed effect is not simply elevated XEB. It is elevated Madmartigan-reference XEB in the raw exact-kernel circuit, combined with suppressed or weakened Madmartigan-reference XEB in matched native-bridge controls that nevertheless preserve their own reference structure.

### 4.3 Heavy Output Generation: HOG

HOG measures how much observed probability mass lands on bitstrings whose ideal probabilities exceed the ideal median. Values above 0.5 indicate heavy-output preference relative to the reference distribution. As with XEB, HOG is reference-dependent.

### 4.4 Shannon Entropy

Shannon entropy measures the spread of the observed tile distribution. For 16-bit tile outputs, the maximum possible entropy is 16 bits, but with 4096 shots, observed entropy is constrained by sampling sparsity. The raw and control distributions generally occupied an entropy window around 11.84–11.91 bits per 16-bit tile, indicating broad NISQ-limited structured distributions rather than trivial single-state collapse.

### 4.5 Inverse Participation Ratio: IPR

IPR estimates the effective number of populated states. Across the bridged benchmark and controls, IPR values typically clustered in the low-to-mid thousands. Similar entropy/IPR windows across raw and controls indicate similar distributional spread, but not necessarily the same reference identity.

### 4.6 Top-8 Overlap

Top-8 overlap counts whether the hardware’s top eight observed bitstrings intersect the ideal top eight bitstrings. At 4096 shots over a 65,536-state tile space, exact top-8 overlap is stringent and noisy. It is useful as supporting evidence but should not be treated as the sole performance indicator.

## 5 Native-Bridge Physical Layout

The native-bridge benchmark retained the six T6 rank-2 tile paths from the strongest tiled campaign:

Tile 0: [7, 8, 9, 10, 11, 18, 31, 32, 33, 34, 35, 19, 15, 14, 13, 12]  
Tile 1: [147, 148, 149, 150, 151, 138, 131, 132, 133, 134, 135, 139, 155, 154, 153, 152]  
Tile 2: [23, 22, 21, 36, 41, 42, 43, 44, 45, 46, 47, 57, 67, 66, 65, 56]  
Tile 3: [92, 91, 98, 111, 110, 109, 118, 129, 128, 127, 126, 125, 108, 107, 106, 97]  
Tile 4: [53, 54, 55, 59, 75, 74, 73, 72, 71, 70, 69, 78, 89, 88, 87, 86]  
Tile 5: [85, 84, 83, 96, 103, 102, 101, 116, 121, 122, 123, 136, 143, 142, 141, 140]

This produced 96 active qubits embedded in a 156-qubit measured circuit object. The circuit execution was global, while the scoring was regional:

The circuit was global; the scoring was regional; the bridge layer made it cross-region coupled rather than purely tiled.

## 6 Native Cross-Region Bridge Layer

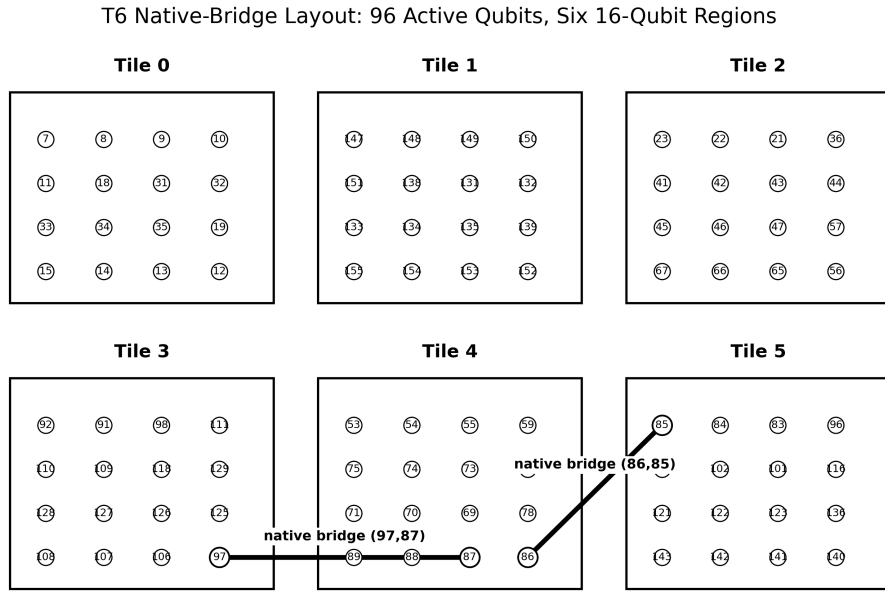
Topology extraction identified 94 active local edges, 92 intra-region active edges, and two cross-region active edges. The selected native bridge pairs were:

Local bridge pairs:  $[(63, 78), (79, 80)]$

Physical bridge pairs:  $[(97, 87), (86, 85)]$

The bridge count was therefore two because the selected active 96-qubit layout exposed two native cross-region edges. This was a conservative design choice. Forcing additional non-native bridges would have introduced routed coupling overhead and potentially confounded the interpretation.

The bridge layer was inserted after Phase IV and before the final BSCM clamp region. This created a minimal native cross-region coupling condition while preserving the exact proven tile kernel.



Single 156-qubit hardware execution; 96 active qubits; regional 16-qubit scoring. Native cross-region bridges connect Tile 3↔4 and Tile 4↔5 via physical pairs (97,87) and (86,85).

Figure 1: T6 native-bridge layout schematic. The benchmark used six 16-qubit tile regions embedded in a single 156-qubit hardware execution, with 96 active qubits and two available native cross-region bridge pairs: physical pairs (97,87) and (86,85). The bridge layer connects Tile 3 to Tile 4 and Tile 4 to Tile 5. The circuit execution was global, while scoring was performed regionally at the 16-qubit tile-projection level.

## 7 Raw Exact-Kernel Native-Bridge Benchmark Configuration

The raw native-bridge benchmark was configured as follows:

Backend: IBM Marrakesh

Total measured qubits: 156

Active qubits: 96

Tiles: 6

Tile size: 16  
Madmartigan reference seed: 1337  
Shots: 4096  
QEC: none  
Post-selection: none  
Native bridge enabled: yes  
Native physical bridge pairs: (97,87), (86,85)  
Full 156-qubit statevector claim: none  
Per-tile ideal reference: 16-qubit seed-1337 Madmartigan distribution

The transpiled profile was:

Depth: 654  
Size: 6546  
SX: 2653  
RZ: 2496  
CZ: 1241  
Measure: 156  
Barrier: 72

This was not a shallow circuit, not a simulation-only circuit, and not a post-selected circuit. It was a real 96-active-qubit, 156-measured-qubit native-bridged hardware execution with more than one thousand CZ gates.

## 8 Raw Native-Bridge Hardware Results

Across five hardware executions, the raw exact-kernel native-bridge circuit preserved the Madmartigan-reference band.

Run-level summaries were:

Run 1:  
meanXEB = 0.905707 | meanHOG = 0.634888 | meanEntropy = 11.8877 | meanIPR = 3666.56

Run 2:  
meanXEB = 1.163848 | meanHOG = 0.661662 | meanEntropy = 11.8824 | meanIPR = 3645.30

Run 3:  
meanXEB = 1.169863 | meanHOG = 0.657104 | meanEntropy = 11.8894 | meanIPR = 3674.98

Run 4:  
meanXEB = 1.182482 | meanHOG = 0.658285 | meanEntropy = 11.8902 | meanIPR = 3672.84

Run 5:  
meanXEB = 1.112927 | meanHOG = 0.650635 | meanEntropy = 11.8834 | meanIPR = 3648.41

Across all raw native-bridge runs:

Tile-level observations: 30  
Mean XEB: 1.106965  
Mean HOG: 0.652515

Mean entropy: 11.886623  
Mean IPR: 3661.616  
Positive XEB observations: 30/30  
HOG > 0.55 observations: 30/30

The strongest interpretation is not that every tile performed identically. The correct interpretation is that a 96-active-qubit native-bridged, uncorrected hardware execution preserved a repeatable Madmartigan-reference structured-output band under real NISQ execution pressure.

## 9 Control Ladder Overview

The completed native-bridge evidence package contains three major control classes:

1. Exact-scaled generic RCS native-bridge control
2. Phase-scrambled exact-scaled native-bridge control
3. Partial-entanglement exact-scaled native-bridge ablation control

Each control uses dual-reference scoring where applicable:

Own-reference scoring:

Hardware output compared to the control circuit's own ideal reference.

Madmartigan-reference scoring:

The same hardware output compared to the original seed-1337 Madmartigan reference.

This dual-reference structure is critical. It prevents the controls from being dismissed as dead circuits. A strong control may preserve its own structure while failing to reproduce the Madmartigan-specific structure.

## 10 Exact-Scaled Generic RCS Native-Bridge Control

### 10.1 Configuration

The exact-scaled generic RCS native-bridge control used the same T6 rank-2 six-tile layout, the same 96 active qubits, the same 156 measured qubits, the same backend, the same 4096 shots, no QEC, no post-selection, and the same native bridge pairs. The final exact-scaled control was engineered to match the raw benchmark in CZ count and barrier count while using generic randomized RCS-style grammar instead of Madmartigan phase/correlation grammar.

The transpiled profile was:

Depth: 643  
Size: 6203  
SX: 2609  
RZ: 2197  
CZ: 1241  
Measure: 156  
Barrier: 72

This control was tightly matched to the raw circuit:

Raw exact-kernel native-bridge:     depth 654 | CZ 1241 | barriers 72



Generic RCS exact-scaled control: depth 643 | CZ 1241 | barriers 72

## 10.2 Results

The generic RCS control was not dead. It preserved own-reference structure:

Mean ownXEB = 0.868  
Mean ownHOG = 0.628  
Mean entropy = 11.898485  
Mean IPR = 3706.867

However, when scored against the seed-1337 Madmartigan reference, it collapsed to near baseline:

Mean Mad1337RefXEB = 0.053016  
Mean Mad1337RefHOG = 0.491268

## 10.3 Interpretation

The generic RCS control answers the question:

Does same-layout, same-bridge, same-CZ generic random circuit behavior reproduce the Madmartigan reference band?

The answer is no. The same physical layout and bridge burden can preserve a generic control's own structure, but that structure does not align with the seed-1337 Madmartigan reference. This rules out a major class of trivial explanations: the bridged Madmartigan result is not merely caused by layout, bridge placement, backend bias, or generic same-scale RCS behavior.

# 11 Phase-Scrambled Exact-Scaled Native-Bridge Control

## 11.1 Configuration

The phase-scrambled control was designed as an architecture-adjacent control. Unlike generic RCS, it remained close to the Madmartigan family but scrambled the phase-command structure. It used the same six T6 rank-2 tile paths, the same native bridge pairs, the same backend, 96 active qubits, 156 measured qubits, 4096 shots, no QEC, and no post-selection.

The transpiled profile was:

Depth: 790  
Size: 6710  
SX: 2759  
RZ: 2551  
CZ: 1244  
Measure: 156  
Barrier: 72

This control was somewhat deeper than the raw exact-kernel native-bridge benchmark but closely matched in CZ count, SX/RZ count, bridge placement, and barrier discipline.

## 11.2 Results

The phase-scrambled control preserved own-reference structure, but did not reproduce the Madmartigan reference band.

Run-level summaries were:

Run 1:

```
meanOwnXEB = 0.727776 | meanOwnHOG = 0.619873
meanMad1337XEB = 0.029056 | meanMad1337HOG = 0.501709
```

Run 2:

```
meanOwnXEB = 0.692265 | meanOwnHOG = 0.624349
meanMad1337XEB = -0.027461 | meanMad1337HOG = 0.495402
```

Run 3:

```
meanOwnXEB = 0.679049 | meanOwnHOG = 0.623006
meanMad1337XEB = -0.029673 | meanMad1337HOG = 0.495076
```

Run 4:

```
meanOwnXEB = 0.712009 | meanOwnHOG = 0.627075
meanMad1337XEB = -0.032565 | meanMad1337HOG = 0.492676
```

Run 5:

```
meanOwnXEB = 0.723132 | meanOwnHOG = 0.622843
meanMad1337XEB = -0.018232 | meanMad1337HOG = 0.493083
```

Aggregate values:

Phase-scrambled own-reference:

```
mean XEB = 0.707
mean HOG = 0.623
```

Phase-scrambled Mad1337-reference:

```
mean XEB = -0.015775
mean HOG = 0.495589
```

## 11.3 Interpretation

The phase-scrambled control answers the question:

Does a Madmartigan-adjacent circuit with similar native-bridge burden reproduce the Madmartigan band if the phase-command grammar is scrambled?

The answer is no. This supports the interpretation that the raw Madmartigan signal depends on the specific phase/correlation program, not merely on depth, CZ burden, physical layout, or broad Madmartigan-like skeleton.

## 12 Partial-Entanglement Native-Bridge Ablation Control

### 12.1 Configuration

The partial-entanglement ablation preserved broad Madmartigan phase sections and substantial entangling burden while breaking the exact EBA chain, QMCA collapse spine, SQCA reciprocal lattice, QPSA fanout targets, and BSCM parity/clamp alignment. It used the same six T6 rank-2 tile paths, 96 active qubits, 156 measured qubits, 4096 shots, no QEC, no post-selection, and the same native bridge pairs.

The transpiled profile was:

```
Depth: 483
Size: 7704
SX: 3658
RZ: 2103
CZ: 1787
Measure: 156
Barrier: 72
```

This control was shallower than the raw bridged benchmark because the transpiler found more parallel scheduling, but it was not lighter. It carried a significantly larger CZ burden than the raw benchmark.

### 12.2 Results

The partial-entanglement ablation produced very high own-reference XEB/HOG while retaining only weak-to-moderate Madmartigan-reference overlap.

Run-level summaries were:

```
Run 1:
meanOwnXEB = 3.095341 | meanOwnHOG = 0.758219
meanMad1337XEB = 0.140027 | meanMad1337HOG = 0.546916
```

```
Run 2:
meanOwnXEB = 3.120875 | meanOwnHOG = 0.762980
meanMad1337XEB = 0.142050 | meanMad1337HOG = 0.547119
```

```
Run 3:
meanOwnXEB = 3.182010 | meanOwnHOG = 0.759644
meanMad1337XEB = 0.153738 | meanMad1337HOG = 0.549723
```

```
Run 4:
meanOwnXEB = 3.411360 | meanOwnHOG = 0.768351
meanMad1337XEB = 0.145935 | meanMad1337HOG = 0.550944
```

```
Run 5:
meanOwnXEB = 3.203835 | meanOwnHOG = 0.764404
meanMad1337XEB = 0.170951 | meanMad1337HOG = 0.550741
```

Aggregate values:

Partial-entanglement own-reference:

mean XEB = 3.202684  
mean HOG = 0.762719

Partial-entanglement Mad1337-reference:  
mean XEB = 0.150540  
mean HOG = 0.549089

## 12.3 Interpretation

This was not a clean negative control in the same sense as generic RCS or phase scrambling. It did not collapse entirely to baseline against the Madmartigan reference. Instead, it produced a new structured-output regime.

The central discovery is:

Breaking the exact Madmartigan entanglement pathways does not destroy all QSCE-family structure. It produces a derivative high-attractor operating mode that is strongly preserved against its own reference while only weakly-to-moderately overlapping the original Madmartigan reference.

This reveals two distinguishable QSCE-related regimes:

Raw exact-kernel Madmartigan:  
Reference-specific command-preservation mode.

Partial-entanglement ablation:  
High-gain QSCE-derived attractor mode with different reference identity.

The ablation's high ownXEB/HOG does not mean it beats Madmartigan at being Madmartigan. It means it preserves its own more concentrated ablated reference distribution extremely well. The lower Madmartigan-reference XEB/HOG proves that it is not the same attractor identity as the original Madmartigan band.

# 13 Comparative Summary of Raw and Control Results

## 13.1 Raw Exact-Kernel Native-Bridge Madmartigan

- 96 active qubits
- 156 measured qubits
- Depth 654
- 1241 CZ gates
- Two native cross-region bridges
- 4096 shots
- No QEC
- No post-selection
- Preserved positive Madmartigan-reference structure across all 30 tile-level observations

### 13.2 Exact-Scaled Generic RCS Native-Bridge Control

- Same six physical tile paths
- Same native bridge pairs
- Same 96 active qubits and 156 measured qubits
- Depth 643
- 1241 CZ gates
- Positive own-reference structure
- Near-baseline Madmartigan-reference XEB/HOG
- Rules out same-scale generic RCS as the explanation

### 13.3 Phase-Scrambled Native-Bridge Control

- Same six physical tile paths
- Same native bridge pairs
- Depth 790
- 1244 CZ gates
- Positive own-reference structure
- Near-baseline Madmartigan-reference behavior
- Rules out phase-insensitive architecture-adjacent explanations

### 13.4 Partial-Entanglement Native-Bridge Ablation

- Same six physical tile paths
- Same native bridge pairs
- Depth 483
- 1787 CZ gates
- Very high own-reference XEB/HOG
- Weak-to-moderate Madmartigan-reference overlap
- Reveals a QSCE-derived high-attractor mode rather than a clean negative control

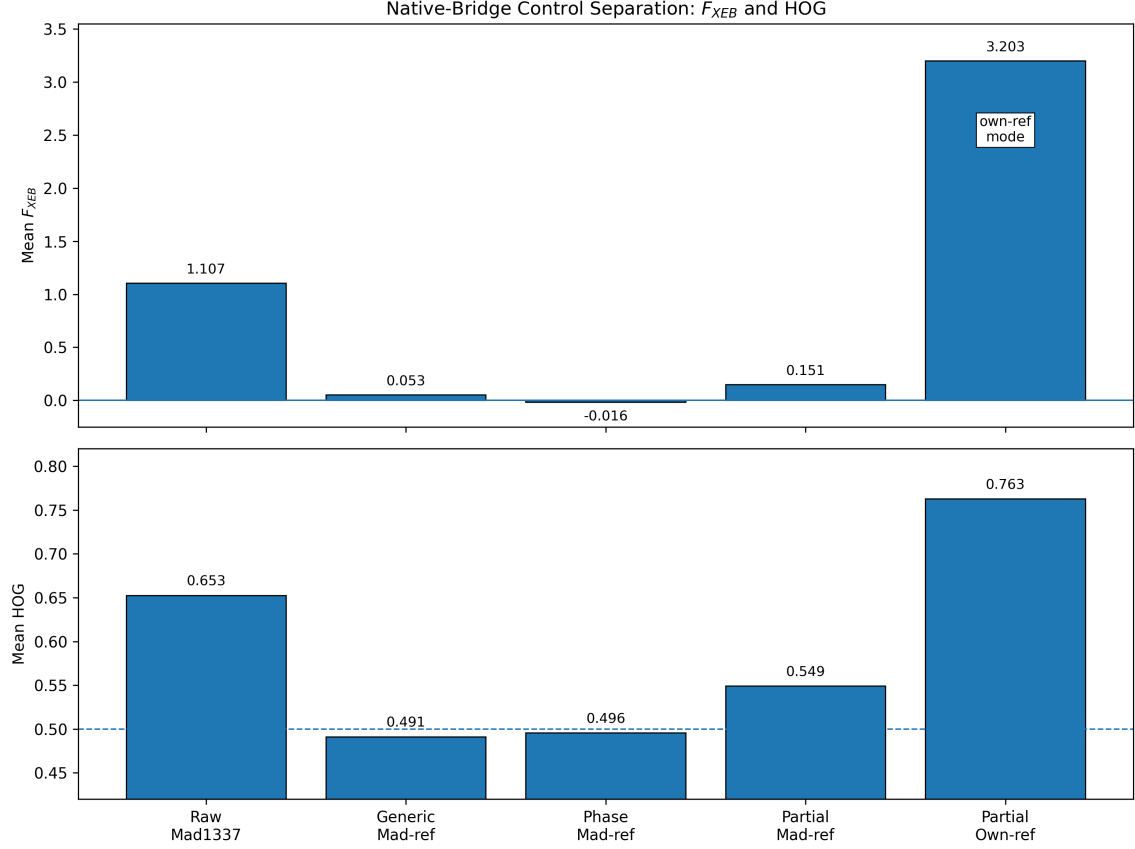


Figure 2: Native-bridge control separation across raw and matched controls. The upper panel reports mean  $F_{XEB}$ ; the lower panel reports mean HOG, with the dashed line marking the  $HOG = 0.5$  baseline. The raw exact-kernel native-bridge Madmartigan circuit preserves elevated Madmartigan-reference  $F_{XEB}$  and HOG. Exact-scaled generic RCS and phase-scrambled controls remain near Madmartigan-reference baseline while preserving their own-reference structure. The partial-entanglement ablation produces a separate high-attractor own-reference mode, shown separately, and should not be interpreted as Madmartigan-reference reproduction.

## 14 Why the Evidence Package Is Scientifically Strong

The native-bridge package is strong because it is not merely a raw result. It includes:

1. Raw exact-kernel native-bridge execution
2. Five-run repeatability
3. Exact-scaled generic RCS control
4. Architecture-adjacent phase-scrambled control
5. Partial-entanglement ablation and attractor-mode discovery
6. Consistent no-QEC/no-post-selection methodology
7. Sparse 4096-shot execution

8. Real IBM hardware execution
9. Per-tile ideal reference metrics
10. Clear distinction between own-reference and Madmartigan-reference scoring
11. Statistical appendix with 95% t-intervals, Welch tests, Cohen’s  $d$ , Mann–Whitney tests, and bootstrap confidence intervals

A reviewer can still ask for independent reproduction, backend replication, and external audit. But as a technical evidence package, the result is mature. It demonstrates not only that the raw signal exists, but that it behaves differently from controls in a reference-dependent way.

## 15 Scientific Significance

The significance of this work is that it moves Madmartigan beyond pure tile replication. The earlier 96-active-qubit tiled benchmark already showed that the original 16-qubit reference band could be replicated across six simultaneous tile paths. The native-bridge benchmark adds the next condition: real cross-region coupling inserted into the 96-active-qubit workload.

The benchmark therefore supports two claims simultaneously:

1. The Madmartigan exact-kernel program can preserve a specific intended reference band under native-bridged NISQ hardware conditions.
2. The broader QSCE/Madmartigan design space can generate multiple structured-output regimes, including a high-attractor derivative mode under partial-entanglement ablation.

For NISQ operational utility, the relevance is that structured, reference-specific quantum output may be usable as a command-bearing, authentication-bearing, or classification-bearing primitive. The result does not prove full fault-tolerant quantum computation. It points to a separate utility class:

Reference-specific structured-output generation on physical NISQ hardware.

## 16 Limitations

The work remains subject to important limitations:

1. It has not yet been independently reproduced by an external lab.
2. It remains backend- and calibration-sensitive.
3. The bridged benchmark uses per-tile 16-qubit reference scoring, not full 96-qubit statevector scoring.
4. It does not prove full 96-qubit statevector fidelity.
5. It does not prove full 96-qubit tomography.
6. It does not prove fault-tolerant computation.
7. The native-bridge count was limited by the available active-topology cross-region edges.
8. The bridged campaign uses fixed Madmartigan seed 1337 and does not yet claim multi-seed bridged generalization.
9. The partial-ablation attractor mode does not yet have assigned operational semantics.

10. The result requires independent audit of bit ordering, projection, reference scoring, and artifact consistency.

These limitations do not erase the result. They define the next scientific steps.

## 17 Recommended Next Steps

### 17.1 Independent Reproduction

The strongest next step is independent reproduction by a technically credible evaluator. The reproduction package should include:

- QPY and QASM3 circuits
- backend metadata
- selected physical tile layout
- bridge topology metadata
- raw counts
- active 96-bit projected counts
- tile-level analysis CSVs
- scoring scripts
- statistical appendix outputs

### 17.2 Backend Replication

The result should be tested on adjacent IBM backends or repeated across calibration windows on Marrakesh to determine whether the effect is backend-specific, layout-specific, or architecture-general.

### 17.3 Seed Extension

The bridged benchmark should eventually test nearby Madmartigan seeds using the same exact-kernel native-bridge discipline. The current paper does not claim bridged multi-seed generalization.

### 17.4 Operational Utility Testing

The raw Madmartigan output bands can be mapped to command labels or classification thresholds. The next operational test would connect the stable output bands to a quantum-to-classical decode pathway and measure classification reliability.

## 18 Final Summary

The Madmartigan native-bridge campaign successfully transformed the earlier tiled 96-active-qubit benchmark into a native-bridged 96-active-qubit structured-output benchmark. The raw exact-kernel native-bridge circuit preserved the seed-1337 Madmartigan reference band across five hardware executions on IBM Marrakesh without QEC, without post-selection, and with only 4096 shots per run.



Exact-scaled generic RCS and phase-scrambled controls preserved their own-reference structure but failed to reproduce the Madmartigan-reference band. Partial-entanglement ablation revealed a separate QSCE-derived high-attractor mode rather than invalidating the original claim.

The final statistically defensible conclusion is:

The T6 Exact-Kernel Native-Bridge Madmartigan benchmark demonstrates repeatable, statistically separated, reference-specific structured-output preservation across a 96-active-qubit native-bridged NISQ workload on IBM Marrakesh, with no QEC and no post-selection. Matched native-bridge controls remain broad and structurally active against their own references, but fail to reproduce the original Madmartigan-reference band.

## A Statistical Significance and Control-Separation Analysis

This appendix reports aggregate statistics computed from the preserved analysis CSVs in the bridged Madmartigan reproducibility bundles. The purpose is not to replace the raw-count audit chain, but to quantify the separation between the T6 Exact-Kernel Native-Bridge Madmartigan executions and the native-bridge control ladder using the tile-level metrics reported throughout the paper. The analysis focuses on  $F_{XEB}$ , HOG, Shannon entropy, and IPR at the 16-qubit tile-projection level.

The present bridged benchmark uses a fixed Madmartigan reference seed, seed 1337. Unlike the earlier tiled benchmark, the present analysis does not claim multi-seed generalization for the bridged campaign. Its claim is fixed-seed repeatability, same-bridge control separation, and mode separation across architecture-adjacent controls.

### A.1 Sparse-Sampling Context

Each tile is a 16-qubit output space with  $2^{16} = 65,536$  possible bitstrings. Each hardware execution used 4096 shots, so the empirical distribution is necessarily sparse. This makes raw representative examples insufficient by themselves. The correct statistical question is whether elevated Madmartigan-reference  $F_{XEB}$  and HOG persist across repeated bridged runs and tiles, and whether same-layout native-bridge controls collapse toward the Madmartigan-reference baseline or separate into distinct non-Madmartigan modes.

The preserved data support this question because each reported hardware run is available as raw counts, metadata, top-string exports, and per-tile analysis CSV. The statistics below therefore treat each tile-level run as one observation in the repeated hardware evidence package. The primary raw dataset contains five hardware runs and six tile projections per run, yielding  $5 \times 6 = 30$  tile-level observations. Each control dataset follows the same  $5 \times 6 = 30$  tile-level observation structure.

### A.2 Circuit and Control Ladder

Table 1 summarizes the transpiled circuit profiles used in the bridged control ladder.

Table 1: Transpiled profile comparison for bridged raw and native-bridge controls.

Circuit	Seed	Depth	CZ	SX	RZ	Barriers
T6 Exact-Kernel Native-Bridge raw	1337	654	1241	2653	2496	72
Exact-scaled generic RCS native-bridge control	1337	643	1241	2609	2197	72
Phase-scrambled exact-scaled native-bridge control	7331	790	1244	2759	2551	72
Partial-entanglement exact-scaled native-bridge control	9137	483	1787	3658	2103	72

### A.3 Aggregate Raw and Control Distributions

Table 2 summarizes the primary  $F_{XEB}$  and HOG distributions. Confidence intervals are 95% t-intervals over the tile-level observations.

Table 2: Primary bridged XEB and HOG summary statistics.

Dataset	n	XEB mean [95% CI]	XEB range	HOG mean [95% CI]	HOG range
96q exact-kernel native-bridge raw	30	1.107 [0.879, 1.335]	0.220 to 2.559	0.653 [0.633, 0.672]	0.571 to 0.776
96q exact-scaled generic RCS control, Mad-ref	30	0.053 [0.010, 0.096]	-0.110 to 0.341	0.491 [0.484, 0.499]	0.453 to 0.535
96q exact-scaled generic RCS control, own-ref	30	0.868 [0.735, 1.001]	0.415 to 1.515	0.628 [0.613, 0.643]	0.576 to 0.706
96q phase-scrambled control, Mad-ref	30	-0.016 [-0.031, -0.001]	-0.077 to 0.070	0.496 [0.492, 0.499]	0.469 to 0.512
96q phase-scrambled control, own-ref	30	0.707 [0.584, 0.830]	0.317 to 1.361	0.623 [0.608, 0.639]	0.558 to 0.706
96q partial-ablation control, Mad-ref	30	0.151 [0.108, 0.193]	-0.140 to 0.274	0.549 [0.539, 0.560]	0.487 to 0.576
96q partial-ablation control, own-ref	30	3.203 [2.506, 3.900]	0.660 to 5.957	0.763 [0.728, 0.798]	0.615 to 0.864

## A.4 Entropy and IPR Support Geometry

Table 3: Entropy and IPR summary statistics for bridged raw and controls.

Dataset	n	Entropy mean [95% CI]	Entropy range	IPR mean [95% CI]	IPR range
96q exact-kernel native-bridge raw	30	11.887 [11.879, 11.894]	11.833 to 11.913	3661.62 [3631.91, 3691.33]	3447.85 to 3758.34
96q exact-scaled generic RCS control, Mad-ref	30	11.898 [11.891, 11.906]	11.866 to 11.934	3706.87 [3680.35, 3733.38]	3586.41 to 3835.67
96q phase-scrambled control, Mad-ref	30	11.905 [11.901, 11.909]	11.879 to 11.929	3732.04 [3716.53, 3747.54]	3634.58 to 3819.95
96q partial-ablation control, Mad-ref	30	11.846 [11.828, 11.863]	11.775 to 11.913	3522.65 [3460.79, 3584.51]	3267.86 to 3760.02

The entropy/IPR values show that the principal controls are not trivial low-entropy failures. The exact-scaled generic RCS and phase-scrambled controls preserve broad support while failing against the Madmartigan reference. The partial-entanglement ablation preserves somewhat lower but still broad support and generates a separate control-own attractor mode.

## A.5 Control-Separation Tests

Table 4 reports raw-versus-control separation for the main bridged comparisons. Cohen’s  $d$  is calculated using the pooled standard deviation, and positive values indicate that the raw bridged Madmartigan distribution is higher than the control distribution. Welch tests and Mann–Whitney tests are reported as distributional checks, not as substitutes for independent external replication. Bootstrap confidence intervals are 95% percentile intervals over the mean difference.

Table 4: Raw-versus-control separation statistics for the bridged benchmark.

Comparison	Metric	Raw mean	Control mean	Diff	95% boot CI	Cohen d	Welch p	MW p
96q exact-kernel bridge raw vs. exact-scaled generic RCS Mad-ref	XEB	1.107	0.053	1.054	[0.851, 1.284]	2.400	1.75e-10	4.98e-11
96q exact-kernel bridge raw vs. exact-scaled generic RCS Mad-ref	HOG	0.653	0.491	0.161	[0.142, 0.182]	4.016	7.37e-18	3.01e-11
96q exact-kernel bridge raw vs. phase-scrambled Mad-ref	XEB	1.107	-0.016	1.123	[0.918, 1.346]	2.596	5.32e-11	3.02e-11
96q exact-kernel bridge raw vs. phase-scrambled Mad-ref	HOG	0.653	0.496	0.157	[0.139, 0.177]	4.106	1.73e-16	3.01e-11
96q exact-kernel bridge raw vs. partial-ablation Mad-ref	XEB	1.107	0.151	0.956	[0.748, 1.189]	2.179	1.57e-09	8.15e-11
96q exact-kernel bridge raw vs. partial-ablation Mad-ref	HOG	0.653	0.549	0.103	[0.083, 0.125]	2.433	3.90e-12	4.05e-11

The strongest negative controls are the exact-scaled generic RCS and phase-scrambled controls. Both preserve healthy own-reference structure while collapsing toward the Madmartigan-reference baseline. The partial-entanglement ablation requires a more nuanced interpretation. It behaves as a mode-separation control: it produces a strong own-reference output mode while retaining only weak-to-moderate overlap with the original Madmartigan seed-1337 band.

## A.6 Control-Own Versus Madmartigan-Reference Separation

Table 5: Control-own reference versus Madmartigan-reference separation.

Comparison	Metric	Own mean	Mad-ref mean	Diff	95% boot CI	Cohen d	Welch p	MW p
generic control own-ref vs. Mad-ref	XEB	0.868	0.053	0.815	[0.687, 0.951]	3.077	7.20e-14	3.02e-11
generic control own-ref vs. Mad-ref	HOG	0.628	0.491	0.137	[0.122, 0.154]	4.265	4.39e-20	3.01e-11
phase-scrambled control own-ref vs. Mad-ref	XEB	0.707	-0.016	0.723	[0.609, 0.844]	3.075	7.29e-13	3.02e-11
phase-scrambled control own-ref vs. Mad-ref	HOG	0.623	0.496	0.128	[0.113, 0.143]	4.153	5.63e-17	3.01e-11
partial-entanglement control own-ref vs. Mad-ref	XEB	3.203	0.151	3.052	[2.392, 3.708]	2.308	7.39e-10	3.02e-11
partial-entanglement control own-ref vs. Mad-ref	HOG	0.763	0.549	0.214	[0.178, 0.248]	3.103	7.66e-14	3.00e-11

The generic and phase-scrambled controls are strong evidence against a hardware/layout-only explanation: both preserve their own broad-support output structure, but their Madmartigan-reference HOG remains near 0.5. The partial-entanglement ablation shows a separate QSCE-derived attractor regime.

## A.7 Fixed-Seed Repeatability at Seed 1337

The bridged raw benchmark used Madmartigan seed 1337. Across five hardware executions and six tiles per execution, the raw bridged circuit produced 30 tile-level observations. All 30/30 tile-level  $F_{XEB}$  values are positive, and all 30/30 HOG values are above 0.55.

The exact-scaled generic RCS control likewise produced healthy own-reference structure, with all 30/30 own-reference  $F_{XEB}$  values positive and all 30/30 own-reference HOG values above 0.55. However, against the seed-1337 Madmartigan reference, the exact-scaled generic control produced mean  $F_{XEB} = 0.053$  and mean HOG = 0.491. The phase-scrambled control produced mean Madmartigan-reference  $F_{XEB} = -0.016$  and mean Madmartigan-reference HOG = 0.496. This is the central fixed-seed control-separation result.

## A.8 Partial-Entanglement Ablation Interpretation

The partial-entanglement ablation is not a clean negative control and should not be presented as one. It is a mode-separation control. Across 30 tile-level observations, it produced a very strong own-reference mode, with mean own-reference  $F_{XEB} = 3.203$  and mean own-reference HOG = 0.763. Against the Madmartigan seed-1337 reference, however, it produced mean  $F_{XEB} = 0.151$  and mean HOG = 0.549, far below the raw bridged Madmartigan band.

This indicates that breaking the exact Madmartigan command-routing pathways does not necessarily destroy all structure. Instead, the circuit can enter a separate QSCE-derived high-attractor regime. That is consistent with earlier tiled partial-entanglement behavior and strengthens the interpretation that the design family contains multiple structured-output modes.

## A.9 Sparse-Sampling Robustness Interpretation

The sparse-sampling objection is not answered by a single large  $F_{XEB}$  value. It is answered by repeatability and control separation. Across the preserved bridged CSVs, elevated Madmartigan-reference  $F_{XEB}$  and HOG recur across five hardware executions and all six tile projections. Exact-scaled generic RCS and phase-scrambled controls preserve their own reference structure but collapse toward Madmartigan-reference baseline. The partial-entanglement ablation produces a different high-attractor own-reference mode with weaker Madmartigan-reference overlap.

Therefore, the statistically defensible conclusion is not that sparse sampling is impossible, nor that the results prove full 96-qubit tomography, full 96-qubit statevector fidelity, or fault-tolerant computation. The defensible conclusion is narrower: the observed bridged Madmartigan-reference elevation is repeatable, reference-specific, and strongly separated from same-layout native-bridge controls in the preserved tile-level data.

# B Circuit Serialization and Reproducibility Manifest

The reproducibility archive contains the artifacts needed to audit the reported circuit construction, hardware execution, raw-count storage, and analysis pipeline. Table 6 summarizes the artifact classes detected across the four bridged benchmark bundles.

The archive includes serialized QPY circuits, QASM3 exports, raw counts, metadata, backend snapshots, job-result representations, analysis JSON summaries, top-string CSVs, and tile-level analysis CSVs. This supports the intended audit path:

```
QPY / QASM3 circuit artifact
->
```

Table 6: Reproducibility artifact manifest summary for bridged raw and control bundles.

Artifact class	Files	MB
analysis_csv	20	0.08
analysis_json	20	0.02
backend_snapshot	4	0.00
job_result	60	1.59
manifest	4	0.01
metadata_csv	12	0.03
metadata_json	28	0.10
other	12	0.00
qasm_export	8	0.63
qpy_circuit	8	1.78
raw_counts	40	21.25
top_strings_csv	40	0.36

backend metadata and transpilation profile

->

hardware counts

->

tile-level projection

->

ideal-reference comparison

->

XEB / HOG / entropy / IPR metrics

->

reported bridged benchmark claim

The manifest CSV accompanying this appendix lists each file path, artifact class, top-level campaign folder, file extension, and byte size.

## C Full Tile-Level Run Tables

The complete tile-level audit table is preserved in the reproducibility bundle as:

`appendix_C_full_tile_level_run_tables.csv`

This file contains every tile-level observation used in the statistical appendix, including run index, tile index, dataset kind, reference type,  $F_{XEB}$ , HOG, Shannon entropy, IPR, positive-XEB flag, and HOG-threshold flag.

For readability, the main paper does not reproduce the full table inline. The complete CSV should be treated as the authoritative audit table for tile-level metrics. The companion file:

`appendix_C_run_level_summary.csv`

provides run-level means, maxima, and threshold counts for each raw and control dataset.

## D Native Bridge Topology and Transpiled Profiles

This appendix documents the physical tile layout, active-edge topology, native bridge selection, and transpiled circuit profiles used in the bridged benchmark and control ladder. The complete machine-readable

topology tables are preserved as:

`appendix_D_native_bridge_topology_edges.csv`  
`appendix_D_bridge_topology_summary.csv`  
`appendix_D_tile_paths.csv`  
 and `appendix_D_transpiled_profile_comparison.csv`.

## D.1 T6 Rank-2 Tile Paths

All T6 rank-2 physical tile paths used for the native-bridge benchmark are listed below.

Table 7: T6 rank-2 physical tile paths used for the native-bridge benchmark.

Tile	Physical qubits
0	[7, 8, 9, 10, 11, 18, 31, 32, 33, 34, 35, 19, 15, 14, 13, 12]
1	[147, 148, 149, 150, 151, 138, 131, 132, 133, 134, 135, 139, 155, 154, 153, 152]
2	[23, 22, 21, 36, 41, 42, 43, 44, 45, 46, 47, 57, 67, 66, 65, 56]
3	[92, 91, 98, 111, 110, 109, 118, 129, 128, 127, 126, 125, 108, 107, 106, 97]
4	[53, 54, 55, 59, 75, 74, 73, 72, 71, 70, 69, 78, 89, 88, 87, 86]
5	[85, 84, 83, 96, 103, 102, 101, 116, 121, 122, 123, 136, 143, 142, 141, 140]

## D.2 Active Topology and Native Bridge Selection

Topology extraction identified 94 active local edges inside the selected 96-qubit physical path: 92 intra-region active edges and 2 cross-region active edges. The selected native bridges were therefore the two available active-topology cross-region edges:

Local bridge pairs: [(63, 78), (79, 80)]

Physical bridge pairs: [(97, 87), (86, 85)]

The bridge count was two because the selected active 96-qubit layout exposed two native cross-region edges. This is the conservative native-bridge condition: the benchmark uses the cross-region couplers actually present in the selected physical layout rather than forcing non-native routed couplings.

Table 8: Native bridge topology summary across raw and control circuits.

Campaign	Active edges	Intra-region	Cross-region	Physical bridges
raw	94	92	2	[[97, 87], [86, 85]]
generic	94	92	2	[[97, 87], [86, 85]]
phase	94	92	2	[[97, 87], [86, 85]]
partial	94	92	2	[[97, 87], [86, 85]]

### D.3 Transpiled Profile Comparison

Table 9: Transpiled profile comparison for the bridged raw circuit and native-bridge controls.

Circuit	Depth	CZ	SX	RZ	Barriers	Native bridges
T6 Exact-Kernel Native-Bridge raw	654	1241	2653	2496	72	[[97, 87], [86, 85]]
Exact-scaled generic RCS native-bridge control	643	1241	2609	2197	72	[[97, 87], [86, 85]]
Phase-scrambled exact-scaled native-bridge control	790	1244	2759	2551	72	[[97, 87], [86, 85]]
Partial-entanglement exact-scaled native-bridge control	483	1787	3658	2103	72	[[97, 87], [86, 85]]

### D.4 Active Edge Audit Table

The file `appendix_D_native_bridge_topology_edges.csv` lists all 94 active local edges with local endpoints, physical endpoints, region assignments, edge type, and a selected-bridge flag. This provides an audit path from the selected six-tile physical path to the two native cross-region bridge operations used in the benchmark.

## E Control Construction Details

This appendix documents the construction logic for the raw exact-kernel native-bridge circuit and the three native-bridge controls. The purpose is to make clear that the controls were not arbitrary or dead circuits. Each control preserved the same physical layout, native bridge-selection discipline, 96 active qubits, 156 measured qubits, 4096-shot execution, no-QEC/no-post-selection methodology, and per-tile 16-qubit ideal-reference scoring. The controls differed in the circuit grammar being tested.

The complete machine-readable summary is preserved as `appendix_E_control_construction_summary.csv`.

Table 10: Control construction summary for the bridged benchmark.

Circuit	Seed	Purpose	Construction logic
T6 Exact-Kernel Native-Bridge raw	1337	Preserve exact 16-qubit Madmartigan tile kernel while inserting minimal available native cross-region bridge operations.	Exact Madmartigan seed-1337 tile kernel replicated across six T6 rank-2 regions.
Exact-scaled Generic RCS Native-Bridge control	1337	Same-layout, same-bridge, same-CZ/barrier generic comparator.	Replaces Madmartigan phase/correlation grammar with seeded generic randomized phase/entangling choices while preserving scale and support-geometry burden.
Phase-scrambled Exact-Scaled Native-Bridge control	7331	Architecture-adjacent control preserving skeleton and bridge burden while disrupting phase-command grammar.	Preserves Madmartigan skeleton and phase-slot schedule; applies deterministic phase/rotation perturbations using <code>PHASE_SCRAMBLE_SEED=7331</code> .
Partial-entanglement Exact-Scaled Native-Bridge ablation	9137	Mode-separation ablation preserving broad skeleton but breaking exact command pathways.	Preserves broad Madmartigan section skeleton and phase-slot schedule; performs topology-preserving partial-entanglement ablation, wrong-pair routing, parity disruption, and BSCM/QPSA command-coupling disruption.

### E.1 Raw Exact-Kernel Native-Bridge Circuit

The raw circuit preserves the exact original 16-qubit Madmartigan seed-1337 tile kernel across the six T6 rank-2 regions. It adds the two available native cross-region bridge operations after Phase IV and before the BSCM clamp region. This tests whether the previously validated tiled kernel survives minimal native cross-region coupling rather than remaining a purely tiled execution.

## E.2 Exact-Scaled Generic RCS Native-Bridge Control

The generic RCS control is the same-layout, same-bridge, same-CZ/barrier comparator. It is not the Madmartigan kernel. It replaces Madmartigan phase/correlation grammar with seeded generic randomized phase and entangling choices while preserving the same six physical tile paths, same native bridge pairs, same 96 active qubits, same 156 measured qubits, same shots, no-QEC/no-post-selection discipline, and per-tile ideal-reference scoring. It is scored both against its own ideal reference and against the Madmartigan seed-1337 reference.

## E.3 Phase-Scrambled Exact-Scaled Native-Bridge Control

The phase-scrambled control is architecture-adjacent. It preserves the Madmartigan skeleton and phase-slot schedule, but applies deterministic phase/rotation perturbations using phase-scramble seed 7331. This tests whether the broad Madmartigan-like skeleton and native-bridge burden are sufficient to reproduce the Madmartigan band once the reference-aligned phase grammar is disrupted.

## E.4 Partial-Entanglement Exact-Scaled Native-Bridge Ablation

The partial-entanglement ablation is a mode-separation control, not a clean negative control. It preserves the broad Madmartigan section skeleton and substantial two-qubit pressure, but breaks exact command pathways using partial-entanglement seed 9137. It disrupts exact EBA/QMCA/SQCA/QPSA/BSCM command routing, wrong-pair alignment, parity alignment, and command-coupling structure. It is scored against both its own partial-ablation reference and the original Madmartigan seed-1337 reference.

## E.5 Interpretation Discipline

The control ladder supports three distinct conclusions:

1. The exact-scaled generic RCS control shows that same-layout, same-bridge, same-CZ generic random-circuit behavior does not reproduce the Madmartigan-reference band.
2. The phase-scrambled control shows that a Madmartigan-adjacent skeleton does not reproduce the Madmartigan-reference band when the phase-command grammar is scrambled.
3. The partial-entanglement ablation shows that disrupting exact command pathways can produce a separate QSCE-derived high-attractor mode, but not the original Madmartigan-reference band.

Thus, the controls are not interpreted as “raw worked and controls died.” The more precise interpretation is that the controls remained active against their own references but did not reproduce the reference identity of the raw exact-kernel Madmartigan circuit.